

Warping and tearing of misaligned circumbinary disks around eccentric SMBH binaries

K. Hayasaki,^{a,1} B. W. Sohn,^{a,b} A. T. Okazaki,^c T. Jung^a
G. Zhao^a and T. Naito^d

^aKorea Astronomy and Space Science Institute, Daedeokdaero 776, Yuseong, Daejeon 305-348, Korea

^bDepartment of Astronomy and Space Science, University of Science and Technology, 217 Gajeong-ro, Daejeon, Korea

^cFaculty of Engineering, Hokkai-Gakuen University, Toyohira-ku, Sapporo 062-8605, Japan

^dFaculty of Management Information, Yamanashi Gakuin University, Kofu, Yamanashi 400-8575, Japan

E-mail: kimi@kasi.re.kr, bwsohn@kasi.re.kr, okazaki@lst.hokkai-s-u.ac.jp,
thjung@kasi.re.kr, gyzhao@kasi.re.kr, tsuguya@ygu.ac.jp

Abstract. We study the warping and tearing of a geometrically thin, non-self-gravitating disk surrounding binary supermassive black holes on an eccentric orbit. The circumbinary disk is significantly misaligned with the binary orbital plane, and is subject to the time-dependent tidal torques. In principle, such a disk is warped and precesses, and is torn into mutually misaligned rings in the region, where the tidal precession torques are stronger than the local viscous torques. We derive the tidal-warp and tearing radii of the misaligned circumbinary disks around eccentric SMBH binaries. We find that in disks with the viscosity parameter α larger than a critical value depending on the disk aspect ratio, the disk warping appears outside the tearing radius. This condition is expressed as $\alpha > \sqrt{H/(3r)}$ for $H/r \lesssim 0.1$, where H is the disk scale height. If $\alpha < \sqrt{H/(3r)}$, only the disk tearing occurs because the tidal warp radius is inside the tearing radius, where most of disk material is likely to rapidly accrete onto SMBHs. In warped and torn disks, both the tidal-warp and the tearing radii most strongly depend on the binary semi-major axis, although they also mildly depend on the other orbital and disk parameters. This strong dependence enables us to estimate the semi-major axis, once the tidal warp or tearing radius is determined observationally: For the tidal warp radius of 0.1 pc, the semi-major axis is estimated to be $\sim 10^{-2}$ pc for $10^7 M_{\odot}$ black hole with typical orbital and disk parameters. We also briefly discuss the possibility that central objects of observed warped maser disks in active galactic nuclei are supermassive black hole binaries.

¹Corresponding author.

Contents

1	Introduction	1
2	Tidally driven warping and tearing of a misaligned circumbinary disk	2
2.1	Tidal torques acting on the misaligned circumbinary disk	3
2.2	Tidal warping vs. tearing	7
2.3	Warping and tearing of circumbinary disks in AGNs	9
3	Discussion	11
4	Conclusion	12

1 Introduction

Supermassive black holes (SMBHs) with mass $10^5 M_\odot \lesssim M \lesssim 10^{10} M_\odot$ are considered to reside at the center of most galaxies [1]. Hitherto, SMBHs have been found in 87 galaxies by observing the proper motion of stars bound by the SMBHs or by detecting radiation emitted from gas pulled gravitationally by the SMBHs [2]. H₂O maser emission from active galactic nuclei (AGNs) in spiral galaxies provides a strong tool to measure supermassive black hole (SMBH) masses, because it arises from a rotating disk on a subparsec scale with a nearly Keplerian velocity distribution around a SMBH. Those maser disks have been observed at the centers of NGC 4258 [3], NGC 1068 [4], NGC 3079 [5], the Circinus galaxy [6], UGC 3789 [7], NGC 6323 [8], NGC 2273, NGC 6264, and some more objects [9]. Several maser disks show warped structure at the radii of ~ 0.1 pc [6, 9–11]. From an observational point of view, maser spots on the disk in NGC 4258 are spatially distributed along a line on each side of a central black hole. The SMBH is then thought to be located at the center of a line connecting those two lines by a simple extrapolation, and the disk starts to warp at the innermost maser spot. What mechanism makes the disk warped still remains an open question.

Several scenarios have been proposed for explaining disk warping. Pringle [12] showed that centrally illuminated accretion disks are unstable to warping due to the reaction force of reradiated radiation. Such a radiation-driven warping mechanism has also been applied to explain the disk warping in the context of X-ray binaries [13–16]. If angular momentum vector of an accretion disk around a spinning black hole is misaligned with the spin axis, differential Lense-Thirring torque due to the frame-dragging effect aligns the inner part of the disk with the black-hole equatorial plane. Since the outer part of the disk retains its initial orientation, the resultant disk is warped [17]. This Bardeen-Petterson effect is also considered to be a plausible mechanism for disk warping in maser disks [18]. Moreover, Bregman & Alexander [19] proposed that the warped disk at the center of NGC 4258 is caused by the process of resonant relaxation, which is a rapid relaxation mechanism to exchange angular momentum between the disk and the stars moving under the nearly spherical potential dominated by the SMBH. These mechanisms have been mostly discussed based on the assumption that the central object surrounded by the warped maser disk is a single SMBH.

The tight correlation between the mass of SMBHs and the mass or luminosity of the bulge of their host galaxies ([20–23]; see also [2] for a review) suggests that the SMBH at the center of each galaxy should have evolved toward coalescence in a merged galaxy. If this is

the case, a binary of SMBHs on a parsec or subparsec scale should be formed in a merged galactic nucleus before two black holes finally coalesce, yet no SMBH binaries have clearly been identified so far despite some claims (see [24, 25] for reviews and references therein).

A possible link between the presence of SMBH binaries and the warping of observed maser disks has been studied by Hayasaki et al. [26] (hereafter, H14a). They have, for simplicity, assumed that the circumbinary disk is initially aligned with the binary orbital plane. However, the angular momentum vector of the circumbinary disk does not always coincide with that of the binary orbital angular momentum, because the orientation of the circumbinary disk is primarily due to the angular momentum distribution of the gas supplied to the central region of AGNs. Therefore, the orientation of the circumbinary disk plane is expected to be distributed randomly with respect to the binary orbital plane. The formation of such a misaligned circumbinary disk around SMBH binaries has been numerically examined by Dunhill et al. [27]. Hayasaki et al. [28] have investigated the accretion process from misaligned circumbinary disks onto SMBHs in eccentric orbits.

Regarding the misaligned disk structure, the inner part of the circumbinary disk tends to align with the binary orbital plane, because the tidal precession torque is stronger than the shear viscous torque in the vertical direction, whereas the outer part tends to retain the original state because the tidal precession torque is weaker than the vertical viscous torque. This is the origin of disk warping [29–31].

On the other hand, Nixon et al. [32] have recently proposed that the circumbinary disk is broken into mutually misaligned rings, if the tidal precession torque is stronger than the local horizontal viscous torque in circular SMBH binaries. However, little is known about the relationship between disk tearing and warping in eccentric SMBH binaries.

In this paper, we examine the tidally driven warping and tearing of misaligned circumbinary disks around eccentric SMBH binaries. In Section 2, we describe the tidal torques originating from a time-dependent binary potential and derive the tidal warp radius of the misaligned circumbinary disk. In Section 3, we discuss a possibility that the observed warping of maser disks in several AGNs is caused by the tidal effect of SMBH binaries. Finally, Section 4 summarises our scenario.

2 Tidally driven warping and tearing of a misaligned circumbinary disk

Let us consider the torques from the binary potential acting on the circumbinary disk, which is misaligned with the binary orbital plane, surrounding two black holes in a binary on a eccentric orbit. Figure 1 illustrates a schematic picture of the setting of our model; binary black holes orbiting each other are surrounded by a misaligned circumbinary disk. The binary is put on the x - y plane with its center of mass being at the origin in the Cartesian coordinate. The masses of the primary and secondary black holes are represented by M_1 and M_2 , respectively, and $M = M_1 + M_2$. We put a circumbinary disk around the origin. The unit vector of specific angular momentum of the disk is expressed by (e.g. Pringle [12])

$$\boldsymbol{l} = \cos \gamma \sin \beta \hat{x} + \sin \gamma \sin \beta \hat{y} + \cos \beta \hat{z}, \quad (2.1)$$

where β is the tilt angle between the circumbinary disk plane and the binary orbital plane, and γ is the azimuth of tilt. Here, \hat{x} , \hat{y} , and \hat{z} are unit vectors in the x , y , and z , respectively.

Table 1. Model parameters

Definition	Symbol
Total black hole mass	M
Primary black hole mass	M_1
Secondary black hole mass	M_2
Schwarzschild radius	$r_S = 2GM/c^2$
Binary mass ratio	$q = M_2/M_1$
Mass ratio parameters	$\xi_1 = q/(1+q), \xi_2 = 1/(1+q)$
Binary semi-major axis	a
Orbital eccentricity	e
Orbital frequency	$\Omega_{\text{orb}} = \sqrt{GM/a^3}$
Orbital period	$P_{\text{orb}} = 2\pi/\Omega_{\text{orb}}$
True anomaly	$f_2 = f_1 + \pi$
Tilt angle	β
Azimuth of tilt	γ
Azimuthal angle	ϕ
Shakura-Sunyaev viscosity parameter	α
Horizontal shear viscosity	ν_1
Vertical shear viscosity	ν_2
Ratio of vertical to horizontal shear viscosities	$\eta = \nu_2/\nu_1$
Mass-to-energy conversion efficiency	ϵ

The position vector of the disk can be expressed by

$$\begin{aligned} \mathbf{r} = & r(\cos \phi \sin \gamma + \sin \phi \cos \gamma \cos \beta)\hat{\mathbf{x}} \\ & + r(\sin \phi \sin \gamma \cos \beta - \cos \phi \cos \gamma)\hat{\mathbf{y}} \\ & - r \sin \phi \sin \beta \hat{\mathbf{z}} \end{aligned} \quad (2.2)$$

where the azimuthal angle ϕ is measured from the descending node. The difference from equation (3) of Paper I is the position vector of each black hole, which is given by

$$\mathbf{r}_i = r_i \cos f_i \hat{\mathbf{x}} + r_i \sin f_i \hat{\mathbf{y}} \quad (i = 1, 2), \quad (2.3)$$

where $f_2 = f_1 + \pi$ is the true anomaly and r_i is written as

$$r_i = \xi_i \frac{a(1 - e^2)}{1 + e \cos f_i} \quad (2.4)$$

with $\xi_1 \equiv q/(1+q)$ and $\xi_2 \equiv 1/(1+q)$. Here, e is the binary orbital eccentricity, $q = M_2/M_1$ is the binary mass ratio, and $a = a_1 + a_2$ is the binary semi-major axis with $a_1 \equiv \xi_1 a$ and $a_2 \equiv \xi_2 a$. These and other model parameters are listed in Table 1. We also assume that the disk total angular momentum is small compared with the binary angular momentum.

2.1 Tidal torques acting on the misaligned circumbinary disk

The gravitational force on the unit mass at position \mathbf{r} on the circumbinary disk can be written by

$$\mathbf{F}_{\text{grav}} = - \sum_{i=1}^2 \frac{GM_i}{|\mathbf{r} - \mathbf{r}_i|^3} (\mathbf{r} - \mathbf{r}_i) \quad (2.5)$$

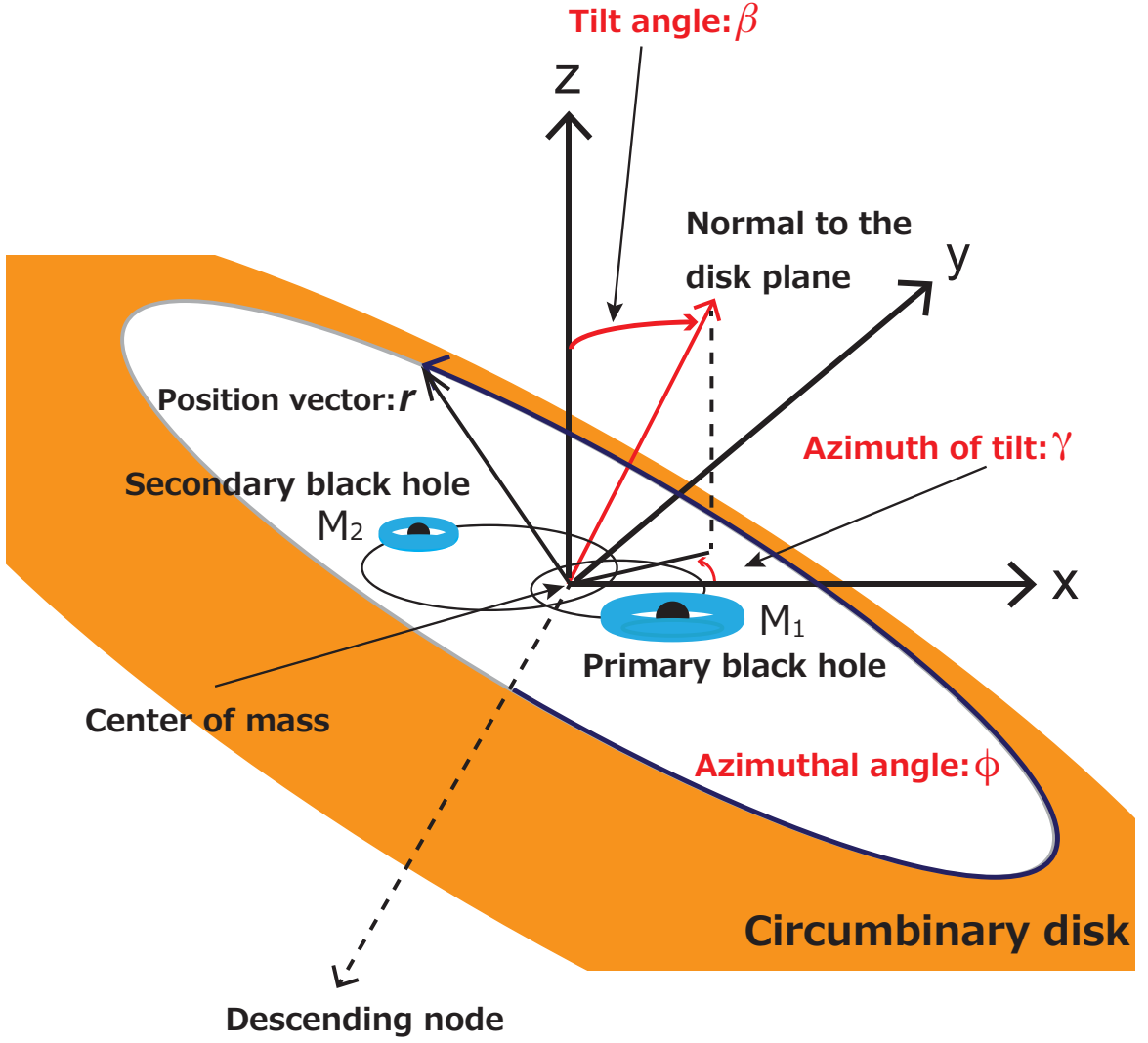


Figure 1. Configuration of a SMBH binary on an eccentric orbit and a circumbinary disk surrounding it. There are two angles (β, γ) which specify the orientation of the disk plane with respect to the binary orbital plane (x - y plane). The azimuthal angle (ϕ) of an arbitrary position on the disk is measured from the descending node.

The corresponding torque is given by

$$\mathbf{t}_{\text{grav}} = \mathbf{r} \times \mathbf{F}_{\text{grav}} = \sum_{i=1}^2 \frac{GM_i}{|\mathbf{r} - \mathbf{r}_i|^3} (\mathbf{r} \times \mathbf{r}_i) \quad (2.6)$$

We consider the tidal warping/precession with timescales much longer than local rotation period of the circumbinary disk. This allows us to use the torque averaged in the azimuthal

direction and over the orbital period:

$$\begin{aligned}
\langle \mathbf{T}_{\text{grav}} \rangle &\approx \frac{1}{4\pi^2} \int_0^{2\pi} \int_0^{2\pi} \mathbf{t}_{\text{grav}} d\phi d(\Omega_{\text{orb}} t) \\
&= \frac{1}{2\pi} \int_0^{2\pi} \left[\frac{1}{2\pi} \int_0^{2\pi} \sum_{i=1}^2 \frac{GM_i(\mathbf{r} \times \mathbf{r}_i)}{|\mathbf{r} - \mathbf{r}_i|^3} d\phi \right] \frac{(1 - e^2)^{3/2}}{(1 + e \cos f_i)^2} df \\
&= \frac{3}{8} \xi_1 \xi_2 \frac{GM}{r} \left(\frac{a}{r} \right)^2 \left[(1 - e^2) \sin \gamma \sin 2\beta \hat{\mathbf{x}} - (1 + 4e^2) \cos \gamma \sin 2\beta \hat{\mathbf{y}} \right. \\
&\quad \left. + 5e^2 \sin 2\gamma \sin^2 \beta \hat{\mathbf{z}} \right], \tag{2.7}
\end{aligned}$$

which is equivalent to equation (7) of Hayasaki et al. [33], where $\Omega_{\text{orb}} = \sqrt{GM/a^3}$ is the angular frequency of the mean binary motion. Here, we used for integration the following relationship:

$$d(\Omega_{\text{orb}} t) = \frac{(1 - e^2)^{3/2}}{(1 + e \cos f_i)^2} df \tag{2.8}$$

and the approximations:

$$|\mathbf{r} - \mathbf{r}_i|^{-3} \approx r^{-3} \left[1 + 3 \frac{\mathbf{r} \cdot \mathbf{r}_i}{r^2} + \mathcal{O}((r_i/r)^2) \right] \tag{2.9}$$

$$(1 + e \cos f_i)^{-4} \approx 1 - 4e \cos f_i + 10e^2 \cos^2 f_i + \mathcal{O}(e^3), \tag{2.10}$$

where $r \gg a$ is adopted for equations (2.9). The magnitude of the specific tidal torque is given by

$$|\langle \mathbf{T}_{\text{grav}} \rangle| = \frac{3}{8} \xi_1 \xi_2 \frac{GM}{r} \left(\frac{a}{r} \right)^2 \Theta(e, \beta, \gamma) \tag{2.11}$$

where $\Theta(e, \beta, \gamma)$ is a function given by

$$\begin{aligned}
\Theta(e, \beta, \gamma) &= \left\{ 4 \left[5e^2(2 + 3e^2) \cos^2 \gamma + (e^2 - 1)^2 \right] \cos^2 \beta \right. \\
&\quad \left. + 25e^4 \sin^2 2\gamma \sin^2 \beta \right\}^{1/2} \sin \beta. \tag{2.12}
\end{aligned}$$

Figure 2 shows dependence of $\Theta(e, \beta, \gamma)$ on the three parameters: orbital eccentricity e , tilt angle β , and azimuth of tilt γ . It is noted from the figure that there are several zeros in $\Theta(e, \beta, \gamma)$, e.g., for $\beta = 0$ and π with any e and γ . Except for these values, $\Theta(e, \beta, \gamma)$ is of the order of one.

By going through the same procedure as for equation (2.7), we obtain the azimuthally-averaged and orbit-averaged tidal potential acting on the misaligned circumbinary disk around

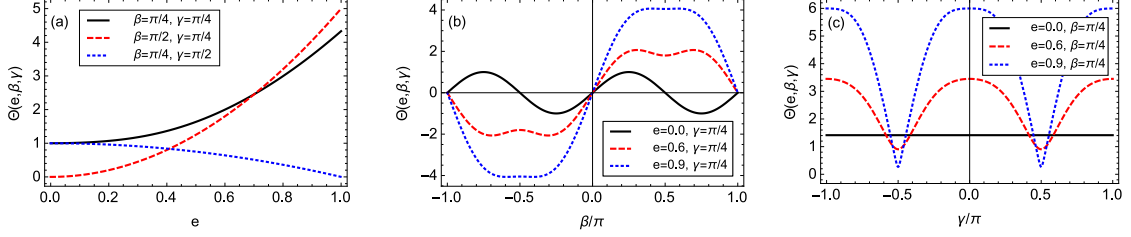


Figure 2. Dependence of $\Theta(e, \beta, \gamma)$ on orbital eccentricity e , tilt angle β , and azimuth of tilt γ . Panel (a); dependence on e with fixed values of β and γ . The solid black, red dashed, and blue dotted lines indicate $\Theta(e, \pi/4, \pi/4)$, $\Theta(e, \pi/2, \pi/4)$, and $\Theta(e, \pi/4, \pi/2)$, respectively. Panel (b); dependence on β with fixed values of e and γ . The solid black, red dashed, and blue dotted lines indicate $\Theta(0.0, \beta, \pi/4)$, $\Theta(0.6, \beta, \pi/4)$, and $\Theta(0.9, \beta, \pi/4)$, respectively. Panel (c); dependence on γ with fixed values of e and β . The solid black, red dashed, and blue dotted lines indicate $\Theta(0.0, \pi/4, \gamma)$, $\Theta(0.6, \pi/4, \gamma)$, and $\Theta(0.9, \pi/4, \gamma)$, respectively.

an eccentric binary:

$$\begin{aligned}
\bar{\Phi} &= \frac{1}{4\pi^2} \int_0^{2\pi} \int_0^{2\pi} - \sum_{i=1}^2 \frac{GM_i}{|\mathbf{r} - \mathbf{r}_i|} d\phi d(\Omega_{\text{orb}} t) \\
&\approx -\frac{GM}{r} \left[1 + \frac{\xi_1 \xi_2}{4} \left[1 + \frac{3}{2} e^2 \right] \left(\frac{a}{r} \right)^2 \right. \\
&\quad \left. - \frac{3\xi_1 \xi_2}{8} (1 - e^2 + 5e^2 \cos^2 \gamma) \sin^2 \beta \left(\frac{a}{r} \right)^2 \right]. \tag{2.13}
\end{aligned}$$

Here, we used for integration equation (2.10) and the following approximation:

$$|\mathbf{r} - \mathbf{r}_i|^{-1} \approx r^{-1} \left[1 + g_i \left(\frac{r_i}{r} \right) + \frac{1}{2} (3g_i^2 - 1) \left(\frac{r_i}{r} \right)^2 + \mathcal{O}((r_i/r)^3) \right], \tag{2.14}$$

where $g_i = \cos \phi \sin(\gamma - f_i) + \sin \phi \cos(\gamma - f_i) \cos \beta$. Since the tidal potential has minima at $\beta = 0$ (alignment) and $\beta = \pi$ (counter-alignment) for arbitrary e and γ , the tidal torques tend to align or counter-align the tilted circumbinary disk with the orbital plane. Note that equation (2.13) is reduced to equation (3) of Hayasaki & Okazaki [34] if $\beta = 0$.

The tidal precession timescale for eccentric binaries is given by

$$\begin{aligned}
\tau_{\text{prec}} &= \frac{|\mathbf{J}|}{|\langle \mathbf{T}_{\text{grav}} \rangle|} = \frac{8}{3} \left(\frac{1}{\xi_1 \xi_2} \right) \left(\frac{r}{a} \right)^2 \frac{1}{\Theta(e, \gamma, \beta)} \frac{1}{\Omega} \\
&= \frac{4}{3\pi} \left(\frac{1}{\xi_1 \xi_2} \right) \left(\frac{r}{a} \right)^{7/2} \frac{1}{\Theta(e, \gamma, \beta)} P_{\text{orb}}
\end{aligned} \tag{2.15}$$

where $\mathbf{J} = r^2 \Omega \mathbf{l}$ with the disk angular frequency $\Omega = GM/r^3$ and $P_{\text{orb}} = 2\pi/\Omega_{\text{orb}}$ are the specific angular momentum and binary orbital period, respectively. Note that the tidal precession timescale depends on the tilt angle and azimuth of tilt for $e \neq 0$. Since the inner edge of the disk is estimated to be $\sim 2a$ [35], the tidal precession timescale is longer than the binary orbital period.

2.2 Tidal warping vs. tearing

There are two types of important viscosities in the circumbinary disk. The first type is the horizontal shear viscosity, ν_1 , which is the viscosity normally associated with accretion disks. The second type is the vertical shear viscosity, ν_2 , which tends to smooth out disk warping when the disk is non-planar. Ogilvie [36] derived the relationship between ν_1 and ν_2 :

$$\eta = \frac{\nu_2}{\nu_1} = \frac{2(1 + 7\alpha^2)}{\alpha^2(4 + \alpha^2)} \quad (2.16)$$

by taking a non-linear effect of the fluid on the warped disk, where η and α are the viscosity ratio parameter and the Shakura-Sunyaev viscosity parameter, respectively. For $\alpha \ll 1$, the above equation is reduced to

$$\eta \approx \frac{1}{2\alpha^2}. \quad (2.17)$$

The global horizontal and vertical viscous timescales for a geometrically thin disk are estimated to be

$$\tau_{\nu_1} = \frac{2r^2}{3\nu_1} \approx \frac{2}{3} \frac{1}{\alpha} \frac{1}{\Omega} \left(\frac{H}{r}\right)^{-2}, \quad (2.18)$$

$$\tau_{\nu_2} = \frac{2r^2}{3\nu_2} \approx \frac{2}{3} \frac{1}{\eta\alpha} \frac{1}{\Omega} \left(\frac{H}{r}\right)^{-2}, \quad (2.19)$$

where $\nu_1 \approx \alpha\Omega H^2$ with the disk scale height H and $\nu_2 \approx \eta\alpha\Omega H^2$. On the other hand, the local horizontal viscous timescale is estimated to be

$$\Delta\tau_{\nu_1} = \frac{2r\Delta r}{3\nu_1} \approx \frac{2}{3} \frac{1}{\alpha} \frac{1}{\Omega} \left(\frac{H}{r}\right)^{-1}, \quad (2.20)$$

where $\Delta r \approx H$ is adopted.

The misaligned circumbinary disk is warped at a radius where the tidal precession timescale is longer than the vertical viscous timescale. We call this radius the tidal warp radius, following Martin et al. [14, 15], who used it in the context of X-ray binaries. The tidal warp radius is given by

$$\frac{R_{\text{warp}}}{r_S} = \left[\frac{3}{8} \frac{\xi_1 \xi_2}{\eta\alpha} |\Theta(e, \beta, \gamma)| \right]^{1/2} \left(\frac{H}{r}\right)^{-1} \left(\frac{a}{r_S}\right), \quad (2.21)$$

Recently, Nixon et al. [32] have proposed that the circumbinary disk is torn into mutually misaligned gas rings if the timescale of the tidal precession, which is strongly differential, is shorter than the local horizontal viscous timescale. The disk tearing occurs at the radius:

$$\frac{R_{\text{tear}}}{r_S} = \left[\frac{1}{4} \frac{\xi_1 \xi_2}{\alpha} |\Theta(e, \beta, \gamma)| \right]^{1/2} \left(\frac{H}{r}\right)^{-1/2} \left(\frac{a}{r_S}\right). \quad (2.22)$$

This reduces to equation (9) of Nixon et al. [32] when $e = 0$. The disk tearing is also confirmed by a three-dimensional Smoothed Particle Hydrodynamics simulations [32]. Inside the tearing radius, the material rapidly accretes onto the central binary, especially, in a

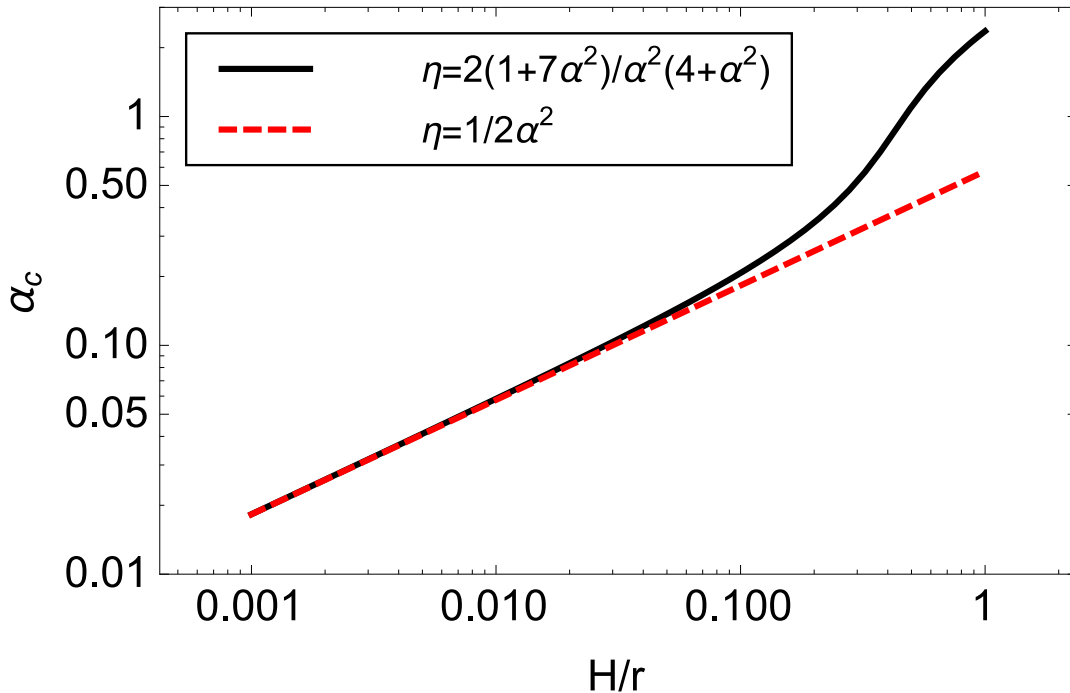


Figure 3. Critical value of viscosity parameter as a function of H/r . The black solid line is the critical value, α_c , of α without approximation to η , whereas the red dashed line is α_c for $\eta \approx 1/(2\alpha^2)$.

retrograde, misaligned circumbinary disk. Therefore, in order for the disk to have a warped structure, R_{warp} must be larger than R_{tear} . This condition is equivalent to

$$\frac{3}{2} \frac{1}{\eta} > \frac{H}{r}. \quad (2.23)$$

This is then rewritten as

$$\alpha > \alpha_c, \quad (2.24)$$

where α_c represents the critical value for the disk viscosity parameter, which is a function of H/r . Figure 3 shows the dependence of α_c on H/r . The red dashed line denotes the critical value of α for $\alpha \ll 1$, which is equal to $\sqrt{H/(3r)}$ obtained by substituting equation (2.17) into equation (2.23). From the figure, we note $\alpha_c = \sqrt{H/(3r)}$ is a good approximation for geometrically thin disks with $H/r < 0.1$. For $\alpha > \alpha_c$, the disk warping occurs outside the tearing radius. Otherwise, no disk warping will occur because there is little disk material at the tidal warp radius, which is inside the tearing radius.

Figure 4 shows the dependence of tidal-warp and tearing radii on the semi-major axis. For a fixed value of $H/r = 0.01$, $\alpha_c \sim 0.06$. We can confirm that the tidal warp radius is larger than the tearing radius for any semi-major axis for $\alpha = 0.1$, whereas it is smaller than the tearing radius for any semi-major axis for $\alpha = 0.01$.

The disk evolves diffusively for $\alpha > H/r$, whereas it does with dispersive wave propagation for $\alpha < H/r$ [37]. For the latter case, the communication time due to wave propagation

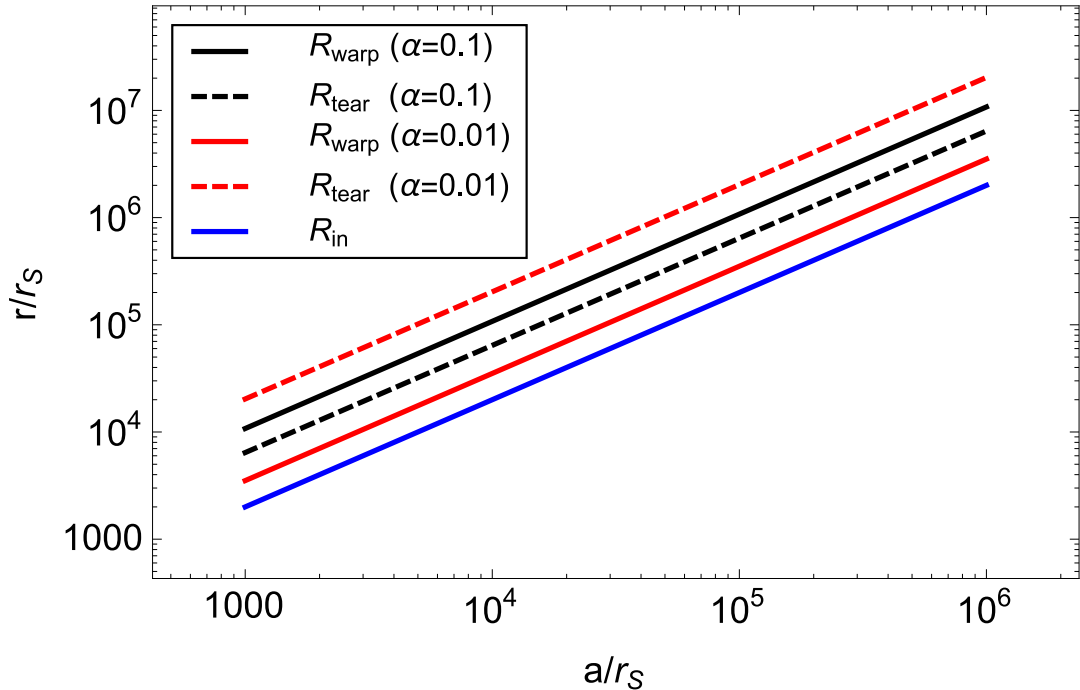


Figure 4. Dependence of tidal-warp and tearing radii on the semi-major axis. The black solid and dashed lines are the tidal-warp and tearing radii for $\alpha > \alpha_c$ case, respectively, whereas the red solid and dashed lines are the tidal-warp and tearing radii for $\alpha < \alpha_c$ case, respectively. Here, $H/r = 0.01$ ($\alpha_c \sim 0.06$) is adopted for each radius. The blue line shows the inner edge radius of the circumbinary disk. The tidal-warp and tearing radii have other common parameters: $M = 10^7 M_\odot$, $q = 0.1$ ($\xi_1 \xi_2 = 10/121$), $e = 0.6$, $\beta = \pi/4$, and $\gamma = \pi/4$, respectively.

is roughly given by $2r/c_s$, where c_s is the local sound speed. The tearing radius is then given by

$$\frac{R_{\text{tear,w}}}{r_s} = \left[\frac{3}{4} \xi_1 \xi_2 |\Theta(e, \beta, \gamma)| \right]^{1/2} \left(\frac{H}{r} \right)^{-1/2} \left(\frac{a}{r_s} \right). \quad (2.25)$$

Comparing this equation with equation (2.21), we obtain, for $\alpha \ll 1$,

$$\frac{R_{\text{warp}}}{R_{\text{tear,w}}} \approx \left(\alpha \frac{r}{H} \right)^{1/2} < 1. \quad (2.26)$$

Thus, no disk warping occurs in a tilted circumbinary disk with $\alpha < H/r$.

2.3 Warping and tearing of circumbinary disks in AGNs

In this section, we apply our model to AGN disks. A gaseous disk around a SMBH in an AGN is surrounded by a dusty torus (e.g. [38]). The grains in the dusty torus is evaporated above the dust sublimation temperature by the irradiation emitted from the central source. The inner radius of the dusty torus should therefore be determined by the dust sublimation radius: $r_{\text{dust}} = 3 \text{ pc} (L/10^{46} \text{ erg s}^{-1})^{1/2} (T_{\text{dust}}/1500 \text{ K})^{-2.8}$, where T_{dust} is the dust sublimation temperature [39]. Assuming that the AGN luminosity is the Eddington

luminosity: $L_{\text{Edd}} \simeq 1.3 \times 10^{38} (M/M_{\odot}) \text{ erg s}^{-1}$, the dust sublimation radius is rewritten as $r_{\text{dust}} = 4.7 \times 10^{-1} (M/10^7 M_{\odot})^{1/2} \text{ pc}$ with the adoption of $T_{\text{dust}} = 1500 \text{ K}$. Since the circumbinary disk should be also inside the dusty torus in our scenario, we assume the disk outer radius and temperature at R_{out} to be given by

$$\frac{R_{\text{out}}}{r_{\text{S}}} \approx 4.8 \times 10^5 \left(\frac{M}{10^7 M_{\odot}} \right)^{-1/2} \quad (2.27)$$

and $T_{\text{out}} = 1500 \text{ K}$, respectively.

Here, we assume that the radial profile of the disk temperature obeys

$$T = T_{\text{out}} \left(\frac{r}{R_{\text{out}}} \right)^s \quad (s < 0), \quad (2.28)$$

where s , R_{out} , and T_{out} are the power law index of the radial profile of the disk temperature, disk outer radius, and temperature at R_{out} , respectively. With the thin disk approximation, the ratio of the disk scale height to radius is then given by

$$\frac{H}{r} = \sqrt{2} \left(\frac{c_{\text{s,out}}}{c} \right) \left(\frac{R_{\text{out}}}{r_{\text{S}}} \right)^{1/2} \left(\frac{r}{R_{\text{out}}} \right)^{(s+1)/2}, \quad (2.29)$$

where $c_{\text{s,out}} = \sqrt{(R_{\text{g}}/\mu)T}$ is the isothermal sound speed at R_{out} with the gas constant R_{g} and molecular weight μ .

Substituting equation (2.29) into equation (2.21), the tidal warp radius is rewritten as

$$\begin{aligned} \frac{R_{\text{warp,AGN}}}{r_{\text{S}}} &= \left[\frac{3}{16} \frac{\xi_1 \xi_2}{\eta \alpha} \Theta(e, \beta, \gamma) \right]^{1/(s+3)} \left(\frac{c}{c_{\text{s,out}}} \right)^{2/(s+3)} \\ &\times \left(\frac{R_{\text{out}}}{r_{\text{S}}} \right)^{s/(s+3)} \left(\frac{a}{r_{\text{S}}} \right)^{2/(s+3)}. \end{aligned} \quad (2.30)$$

Similarly, the tearing radius is rewritten as

$$\begin{aligned} \frac{R_{\text{tear,AGN}}}{r_{\text{S}}} &= \left[\frac{1}{4\sqrt{2}} \frac{\xi_1 \xi_2}{\alpha} \Theta(e, \beta, \gamma) \right]^{2/(s+5)} \left(\frac{c}{c_{\text{s,out}}} \right)^{2/(s+5)} \\ &\times \left(\frac{R_{\text{out}}}{r_{\text{S}}} \right)^{s/(s+5)} \left(\frac{a}{r_{\text{S}}} \right)^{4/(s+5)}. \end{aligned} \quad (2.31)$$

Figure 5 shows characteristic radii of the misaligned circumbinary disk for $e = 0.6$, $q = 0.1$ ($\xi_1 \xi_2 = 10/121$), $M = 10^7 M_{\odot}$, $\alpha = 0.1$ ($\eta \approx 50$), $s = -3/4$, $\beta = \pi/4$, and $\gamma = \pi/4$. The solid and dashed black lines show the tidal warp and tearing radii, respectively. The red solid line shows the radius, which we call the orbital decay radius, where the tidal precession timescale equals the timescale in which the binary orbit decays by the gravitational wave (GW) emission. This orbital decay timescale for an eccentric binary is given by [40]

$$\tau_{\text{gw}} = \frac{5}{8} \frac{1}{\xi_1 \xi_2} \left(\frac{a}{r_{\text{S}}} \right)^4 \frac{r_{\text{S}}}{c} \frac{(1-e^2)^{7/2}}{1 + 73e^2/24 + 37e^4/96} \quad (2.32)$$

Equating equation (2.32) with equation (2.15), we obtain the orbital decay radius:

$$\frac{R_{\text{prec/gw}}}{r_{\text{S}}} = \left[\frac{15}{64\sqrt{2}} \frac{\Theta(e, \beta, \gamma)(1-e^2)^{7/2}}{1 + 73e^2/24 + 37e^4/96} \right]^{2/7} \left(\frac{a}{r_{\text{S}}} \right)^{12/7}. \quad (2.33)$$

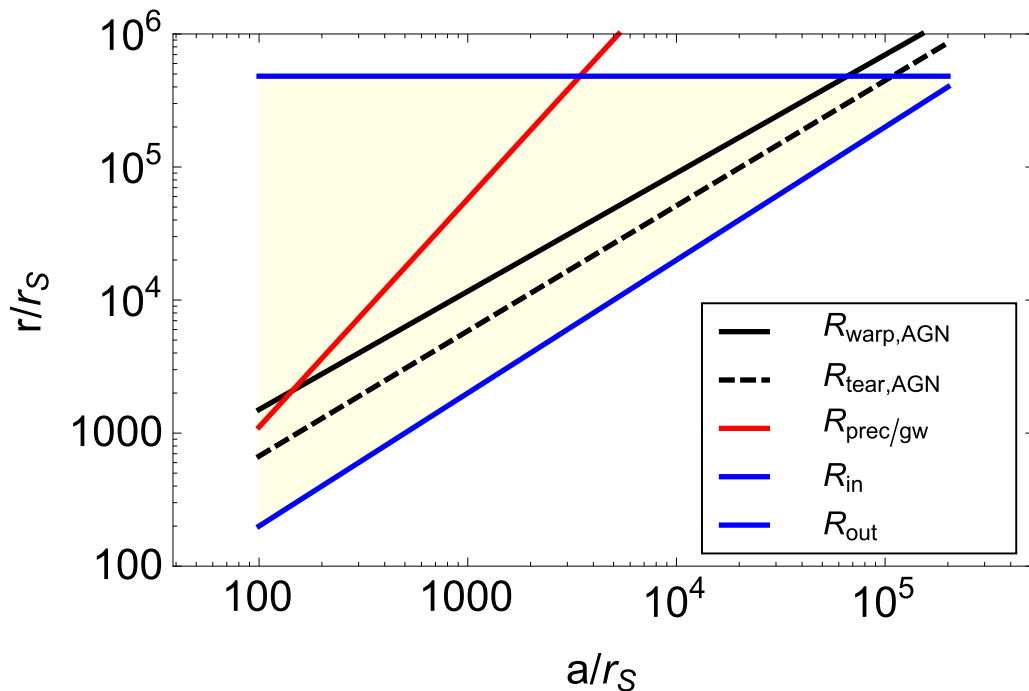


Figure 5. Characteristic radii of the warped and torn circumbinary disk around the SMBH binary on an eccentric orbit for $e = 0.6$, $\alpha = 0.1$ ($\eta \approx 50$), $s = -3/4$, $q = 0.1$ ($\xi_1 \xi_2 = 10/121$), $M = 10^7 M_\odot$, $\beta = \pi/4$, and $\gamma = \pi/4$. The solid and dashed black lines show the tidal warp and tearing radii, respectively. The red solid line shows the orbital decay radius where the tidal precession timescale equals the orbital decay timescale due to the GW emission (see equation (2.33)). While the blue lower line represents the inner radius of the circumbinary disk $r_{\text{in}} \sim 2a$, the blue upper line represents the outer radius of the circumbinary disk $R_{\text{out}}/r_S \approx 4.8 \times 10^4 (M/10^7 M_\odot)^{-1/2}$. The shaded area between the two blue lines represents the whole region of the circumbinary disk.

When it is larger than the tidal warp and tearing radii, the circumbinary disk can be warped and torn before two SMBHs coalesce. Otherwise, two SMBHs coalesce prior to disk warping and tearing. The blue solid lower and upper lines show the inner and outer radii of the circumbinary disk, respectively. The shaded area between the two blue lines shows the whole region of the circumbinary disk.

3 Discussion

In this section, we discuss a possible link between the observational signatures of circumbinary disk warping and tearing and the presence of SMBH binaries. If the warp and/or tearing radii are observationally determined, we can estimate the semi-major axis of the SMBH binary from

equations (2.30) and (2.31) as

$$\frac{a_{\text{warp}}}{r_{\text{S}}} = \left[\frac{16}{3} \left(\frac{\eta\alpha}{\xi_1\xi_2} \right) \frac{1}{\Theta(e, \beta, \gamma)} \right]^{1/2} \left(\frac{c_{\text{s,out}}}{c} \right) \left(\frac{R_{\text{out}}}{r_{\text{S}}} \right)^{-s/2} \times \left(\frac{R_{\text{obs}}}{r_{\text{S}}} \right)^{(s+3)/2}, \quad (3.1)$$

$$\frac{a_{\text{tear}}}{r_{\text{S}}} = \left[4\sqrt{2} \left(\frac{\alpha}{\xi_1\xi_2} \right) \frac{1}{\Theta(e, \beta, \gamma)} \right]^{1/2} \left(\frac{c_{\text{s,out}}}{c} \right)^{1/2} \left(\frac{R_{\text{out}}}{r_{\text{S}}} \right)^{-s/4} \times \left(\frac{R_{\text{obs}}}{r_{\text{S}}} \right)^{(s+3)/4}, \quad (3.2)$$

where R_{obs} shows the tidal warp or tearing radius determined by observations. Figure 6 shows the relationship between this observed radius of disk warping or tearing and the binary semi-major axis. Here, we adopt $\alpha = 0.1$ ($\eta \approx 50$), $s = -3/4$, $q = 0.1$ ($\xi_1\xi_2 = 10/121$), $\beta = \pi/4$, and $\gamma = \pi/4$. The estimated semi-major axes are $a_{\text{warp}} \sim 0.01$ pc and $a_{\text{tear}} \sim 0.02$ pc, although they mildly depend on the orbital eccentricity, binary mass ratio, tilt angle, and azimuth of tilt, except for $\beta = \pi/2, 0$. Because it is observationally more difficult to distinguish between the disk warping and tearing, the actual semi-major axis is likely to be $a_{\text{warp}} \lesssim a \lesssim a_{\text{tear}}$.

There are observational evidences for disk warping in the maser disks at the center of NGC 4258 [10], Circinus [6], NGC 2273, UGC 3789, NGC 6264, and NGC 6323 [9]. The tidally-driven warping or tearing of misaligned circumbinary disks can be one of mechanisms for explaining the warped structure of the maser disks in these systems. Since no observational information is currently available about the warping or tearing radius, we simply assume that these maser disks start to be warped or torn at the innermost maser spot radii. Here, we pick up NGC 4258 case because of the most remarkable example of disk warping among the known maser disk systems. The inner most maser spot radius is 0.17 pc. Assuming that $R_{\text{obs}} = 0.17$ pc, the semi-major axis is estimated to be 1.2×10^{-2} pc. However, it is difficult to distinguish, solely by the current analysis, whether the central object is a single SMBH or such a small-scale SMBH binary. Other independent theoretical and observational approaches are needed.

Probing GWs from individual SMBH binaries with masses $\gtrsim 10^7 M_{\odot}$ with pulsar timing arrays (PTAs; [41, 42]) gives a powerful tool to determine if the central object surrounded by the warped maser disk is a SMBH binary or a single SMBH. For a typical PTA error box ($\approx 40 \text{ deg}^2$) in the sky, the number of interloping AGNs are of the order of 10^2 for more than $10^8 M_{\odot}$ black holes if the redshift range is between 0 and 0.8 (see Figure 1 of Tanaka et al. [43] in detail). As discussed in H14a, even if the observed warped maser disk systems host SMBH binaries, the characteristic amplitudes of GWs from these SMBH binaries are three to four orders of magnitude smaller than the current PTA sensitivity, so that it is unlikely for GWs to be detected from these systems.

4 Conclusion

We have investigated the tidally driven warping and tearing of a geometrically thin, non-self-gravitating circumbinary disk around two SMBHs in a binary on an eccentric orbit, where the

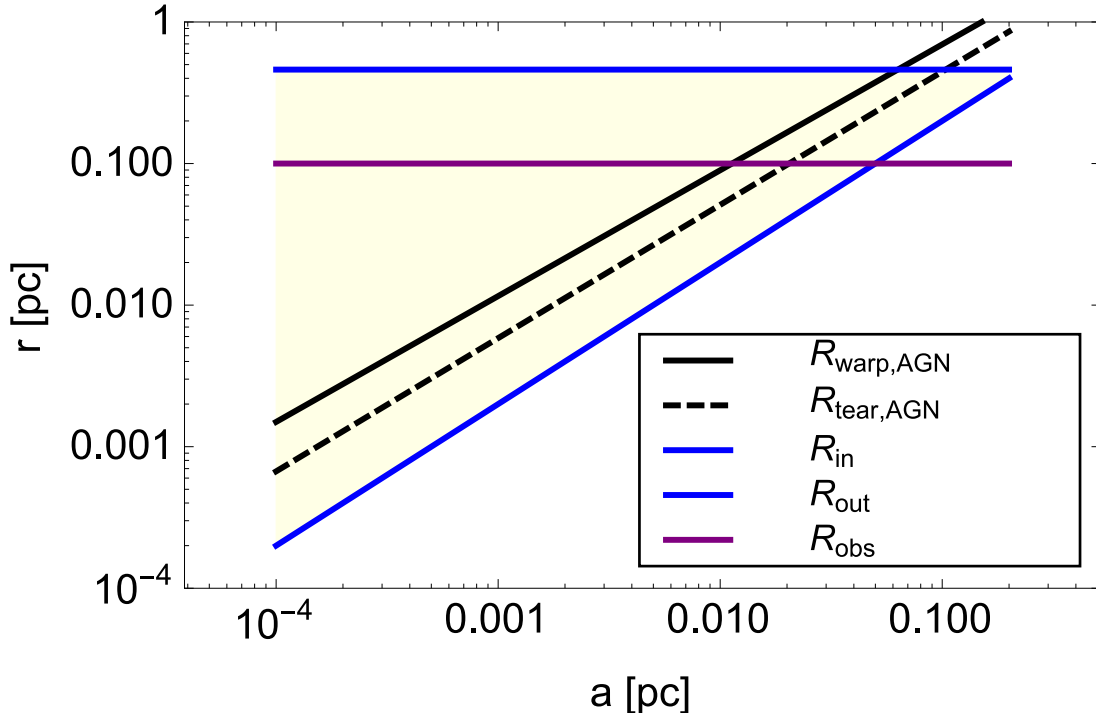


Figure 6. Estimate of a semi-major axis of a SMBH binary by the relationship between the tidal warp and tearing radii and the observed radius, which is shown by the purple solid line. The solid and dashed black lines are, respectively, the tidal-warp and tearing radii of the misaligned circumbinary disk around the eccentric SMBH binary with $e = 0.6$, $\alpha = 0.1$ ($\eta \approx 50$), $s = -3/4$, $q = 0.1$ ($\xi_1 \xi_2 = 10/121$), $M = 10^7 M_\odot$, $\beta = \pi/4$, and $\gamma = \pi/4$. The shaded area between the two blue lines represents the whole region of the circumbinary disk.

original disk plane is misaligned with the binary orbital plane. While tidal torques acting on the tilted circumbinary disk tend to align it with the orbital plane, the viscous torque in the vertical direction tends to retain its original orientation. The disk can then be warped at the tidal warp radius, where the tidal precession timescale equals the vertical viscous timescale. On the other hand, the disk is broken into mutually misaligned rings inside the tearing radius, where the tidal precession timescale equals the local horizontal viscous timescale.

There is a critical value of disk viscosity parameter. If $\alpha > \sqrt{H/(3r)}$ with $H/r \lesssim 0.1$, the tidal warp radius is larger than the tearing radius. Then, the disk tearing first occurs and subsequently disk warping occurs outside the tearing radius. If $\alpha < \sqrt{H/(3r)}$ with $H/r \lesssim 0.1$, only the disk tearing occurs, because the disk material inside the tearing radius is likely to accrete rapidly.

The tidal-warp and tearing radii most strongly depend on the binary semi-major axis, although it mildly depends on the other orbital and disk parameters except for $\beta = 0, \pi$. This strong dependence enables us to estimate the semi-major axis, once the tidal-warp or tearing radius is determined observationally. For the tidal-warp or tearing radius of 0.1 pc, for instance, SMBH binaries with masses of $10^7 M_\odot$ and other typical orbital and disk parameters are estimated to have a binary separation on a 10^{-2} pc scale.

Acknowledgments

They also thank Christopher Nixon for helpful suggestions. K.H. is grateful to Jongsoo Kim for helpful discussions and his continuous encouragement. K.H. would also like to thank the Kavli Institute for Theoretical Physics (KITP) for their hospitality and support during the program on A Universe of Black Holes. B.W.S. and T.H.J. are grateful for support from KASI-Yonsei DRC program of Korea Research Council of Fundamental Science and Technology (DRC-12-2-KASI). This work was also supported in part by the Grants-in-Aid for Scientific Research (C) of Japan Society for the Promotion of Science (23540271 T.N. and K.H.; 24540235 A.T.O. and K.H.).

References

- [1] Kormendy J and Richstone D, *Inward bound—the search for supermassive black holes In galactic nuclei*, *Ann. Rev. Astron. Astr.* **33** (1995) 581
- [2] Kormendy J and Ho L C, *Coevolution (or not) of supermassive black holes and host galaxies*, *Ann. Rev. Astron. Astr.* **51** (2013) 511
- [3] Miyoshi M, Moran J, Herrnstein, J, Greenhill L., Nakai N, Diamond P and Inoue M, *Evidence for a black hole from high rotation velocities in a sub-parsec region of NGC4258* *Nature* **373** (1995) 127.
- [4] Greenhill L J and Gwinn C R, *VLBI Imaging of Water Maser Emission from a Nuclear Disk in NGC 1068* *Astrophys. & Space Sci.* **248** (1997) 261.
- [5] Yamauchi A, Nakai N, Sato N and Diamond P, *Water-Vapor Maser Disk at the Nucleus of the Seyfert 2 Galaxy NGC 3079*, *Publ. Astron. Soc. Jpn.* **56** (2004) 605.
- [6] Greenhill L J, Booth R S and Ellingsen S P, et al., *A warped accretion disk and wide-angle outflow in the inner parsec of the circus galaxy*, *Astrophys. J.* **590** (2003) 162.
- [7] Reid M J, Braatz J A, Condon J J, Greenhill L J, Henkel C and Lo K Y, *The megamaser cosmology project. I. very long baseline interferometric observations of UGC 3789*, *Astrophys. J.* **695** (2009) 287.
- [8] Braatz J, Greenhill L, Reid M, Condon J, Henkel C and Lo K-Y, *Precision cosmology with H₂O megamasers: progress in measuring distances to galaxies in the Hubble flow*, in IAU Symp. 242, *Astrophysical Masers and Their Environments* (Dordrecht: Kluwer) 399 (2007).
- [9] Kuo C Y, et al., *The megamaser cosmology project. III. accurate masses of seven supermassive black holes in active galaxies with circumnuclear megamaser disks*, *Astrophys. J.* **727** (2011) 20.
- [10] Herrnstein J R, Moran J M, Greenhill L J and Trotter A S, *The geometry of and mass accretion rate through the maser accretion disk in NGC 4258*, *Astrophys. J.* **629** (2005) 719.
- [11] Kondratko P T, Greenhill L J and Moran J M, *The parsec-scale accretion disk in NGC 3393*, *Astrophys. J.* **678** (2008) 87.
- [12] Pringle J E, *Self-induced warping of accretion disks*, *Mon. Not. R. Astron. Soc.* **281** (1996) 357.
- [13] Maloney P R and Begelman M C, *The origin of warped, precessing accretions disks in X-ray binaries*, *Astrophys. J.* **491** (1997) L13.
- [14] Martin R. G, Pringle J E and Tout C A, *Alignment and precession of a black hole with a warped accretion disk*, *Mon. Not. R. Astron. Soc.* **381** (2007) 1617.
- [15] Martin R. G, Pringle J E and Tout C A, *The shape of an accretion disk in a misaligned black hole binary*, *Mon. Not. R. Astron. Soc.* **400** (2009) 383.

- [16] Wijers R A M J and Pringle J E, *Warped accretion disks and the long periods in X-ray binaries*, *Mon. Not. R. Astron. Soc.* **308** (1999) 207.
- [17] Bardeen J M and Petterson J A, *The Lense-Thirring effect and accretion disks around Kerr black holes*, *Astrophys. J.* **195** (1975) L65.
- [18] Caproni A, Abraham Z, Livio M and Mosquera Cuesta H J, *Is the Bardeen-Petterson effect responsible for the warping and precession in NGC4258?*, *Mon. Not. R. Astron. Soc.* **379** (2007) 135.
- [19] Bregman M and Alexander T, *Accretion disk warping by resonant relaxation: the case of maser disk NGC 4258*, *Astrophys. J.* **700** (2009) L192.
- [20] McConnell N J and Ma C-P, *Revisiting the scaling relations of black Hole masses and host galaxy properties*, *Astrophys. J.* **764** (2013) 184.
- [21] Ferrarese L and Merritt D, *A Fundamental Relation between Supermassive Black Holes and Their Host Galaxies*, *Astrophys. J.* **539** (2000) L9.
- [22] Gebhardt K, et al., *A Relationship between Nuclear Black Hole Mass and Galaxy Velocity Dispersion* *Astrophys. J.* **539** (2000) L13.
- [23] Magorrian J, et al., *The demography of massive dark objects in galaxy centers*, *Astron. J.* **115** (1998) 2285.
- [24] Komossa S, *Observational evidence for binary black holes and active double nuclei*, *Mem. Soc. Astron. Ital.* **77** (2006) 733.
- [25] Popović, L. Č, *Super-massive binary black holes and emission lines in active galactic nuclei*, *NewAR* 56 (2012) 74.
- [26] Hayasaki K, Sohn B W, Okazaki A, Jung T, Zhao G and Naito T, *Warped circumbinary disks in active galactic nuclei*, *Astrophys. J.* **790** (2014) 62. (H14a)
- [27] Dunhill A C, Alexander R D, Nixon C J and King A R, *Misaligned accretion on to supermassive black hole binaries*, *Mon. Not. R. Astron. Soc.* **445** (2014) 2285.
- [28] Hayasaki K, Saito H and Mineshige S, *Binary black hole accretion flows from a misaligned circumbinary disk*, *Publ. Astron. Soc. Jpn.* **65** (2013) 11.
- [29] Facchini S, Lodato G and Price D J, *Wave-like warp propagation in circumbinary disks ? I. analytic theory and numerical simulations*, *Mon. Not. R. Astron. Soc.* **433** (2013) 2142.
- [30] Lodato G and Facchini S, *Wave-like warp propagation in circumbinary disks ? II. application to KH 15D*, *Mon. Not. R. Astron. Soc.* **433** (2013) 2157.
- [31] Nixon C J, King A R and Pringle J E, *The final parsec problem: aligning a binary with an external accretion disc*, *Mon. Not. R. Astron. Soc.* **417** (2011) L66.
- [32] Nixon C J, King A R and Price D, *Tearing up the disc: misaligned accretion on to a binary*, *Mon. Not. R. Astron. Soc.* **434** (2013) 1946.
- [33] Hayasaki K, Sohn B W, Okazaki A, Jung T, Zhao G and Naito T, *Radiation-driven warping of circumbinary disks around eccentric young star binaries*, *Astrophys. J.* **797** (2014) 68.
- [34] Hayasaki K and Okazaki A T, *A new approach for probing circumbinary disks*, *Astrophys. J.* **691** (2009) L5.
- [35] Artymowicz P and Lubow S H, *Dynamics of binary-disk interaction. 1: resonances and disk gap sizes*, *Astrophys. J.* **421** (1994) 651.
- [36] Ogilvie G, *The non-linear fluid dynamics of a warped accretion disk*, *Mon. Not. R. Astron. Soc.* **304** (1999) 557.
- [37] Papaloizou J C B and Pringle J E, *The time-dependence of non-planar accretion disks*, *Mon. Not. R. Astron. Soc.* **202** (1983) 1181.

- [38] Jaffe W, Ford H C, Ferrarese L, van den Bosch F and OàĀŹConnell R W, *A large nuclear accretion disk in the active galaxy NGC4261*, *Nature* **364** (1993) 213.
- [39] Barvainis R, *Hot dust and the near-infrared bump in the continuum spectra of quasars and active galactic nuclei*, *Astrophys. J.* **320** (1987) 537.
- [40] Peters P C, *Gravitational radiation and the motion of two point masses*, *Phys. Rev.* 136 (1964) B1224.
- [41] Lommen A N and Backer D C, *Using pulsars to detect massive black hole binaries via gravitational radiation: sagittarius A* and nearby galaxies*, *Astrophys. J.* **562** (2001) 297.
- [42] Sesana A, Vecchio A and Volonteri M, *Gravitational waves from resolvable massive black hole binary systems and observations with Pulsar Timing Arrays*, *Mon. Not. R. Astron. Soc.* **394** (2009) 2255.
- [43] Tanaka T, Menou K and Haiman Z, *Electromagnetic counterparts of supermassive black hole binaries resolved by pulsar timing arrays*, *Mon. Not. R. Astron. Soc.* **420** (2012) 705.